Data Repository 2014086

Savi et al., GSA Bullettin

Quantifying sediment supply at the end of the last glaciation: dynamic reconstruction of an alpine debris flow fan

APPENDIX 1 – STRATIGRAPHIC DATA

The 8 cores of the KB-series (KB08 to KB15) are located over a total distance of ca. 1 km (Figure 2) and penetrated different depths, ranging between 21.5 m and 35 m below the surface. From the west to the east, from the external fan to the center, we observe an increasing abundance of coarse-grained material approaching the apex of the modern feeder channel. Here, we measured the section encountered by the drillings KB08 and KB11 at the centimeter scale. For every unit we determined: mean grain size, composition, roundness, wet color (Munsell chart), maximum and mean gravel diameter, upper and lower boundaries, internal coarsening/fining trends and the occurrence of interbeds.

From the results of this description we then interpreted the source of the material, thereby distinguishing between Adige and Zielbach deposits (Fig. 4). The Adige deposits generally consist of fine sand with a polymict composition, silt and clay, arranged as cm-thick layers of alternating grain size, locally graded and organized as fining-up trends. These facies associations are interpreted as overbank deposits of the Adige alluvial plain, locally passing to low-energy/lacustrine environment; the few local coarse pebbly sands could be crevasse splay deposits. The Zielbach deposits generally consist of gravel with a massive fabric, sandy gravel and gravelly sand. Gravels are mainly monolithologic (gneiss), poorly sorted and angular to sub-rounded. The unit boundaries are generally sharp and locally deformed. Large boulders are often found in the cores (size between 20 cm up to 2 m). This facies association is considered to have been deposited by debris-flows. Locally, some pure sand interbeds are encountered sandwiched between Zielbach gravel. This material interpreted as being deposited by Zielbach alluvial processes mainly because the petrographic composition of these sand layers is identical to the sediments found in the modern Zielbach River. More specifically, core KB08 is mainly composed of Adige River deposits, which is in good agreement with the distal location of the core near the edge of the fan (Figs 2 and 4). Between 9.00 m and 10.00 m below the surface, interbeds of reworked-alluvial material from the Zielbach catchment are encountered. Farther down in the drilling, between 21.42 m and 24.00 m, we identified an interval of silt and mud, with very thin laminations, the presence of organic matter sparkled within the material, local peat and traces indicative of oxidations. These sediments are interpreted as pond/lacustrine deposits. At the very end of the core, with a clear and sharp boundary at ca. 26.50 m below the surface, the first deposit correlative to the Zielbach debris-flow is found.

Core KB11 shows alternating deposits derived by the Adige and Zielbach Rivers. From top to bottom, the first 5 m are mainly composed of Zielbach debris-flow material; the lower limit displays a clear erosional boundary. Between 5 m and 14 m, Zielbach and Adige deposits

alternate with different layers and thicknesses. Between 14 m and 22.45 m, only Adige deposits are encountered, while below this depth until the end of the core, at 35 m below the surface, the debris-flow facies predominates.

APPENDIX 2 – FAST AND SLOW BURIAL ^{10}BE CORRECTIONS

Corrections for fast and slow burial have been made on the basis of Schaller et al.'s (2002) method. These authors determined the paleo-denudation rates by calculating the post-depositional ^{10}Be production at a certain depth, considering both nucleonic and a muonic (fast and negative muons) component for the production of ^{10}Be, respectively. We base our corrections on the same formulas (applying a sediment density of 2.2 g/cm^2), modeling different scenarios for fast and slow burial.

The fast burial scenario is explained in the text. The slow burial scenario is simulated considering that the material has been progressively buried, with a rate that corresponds to the sedimentation rates calculated for the Adige River. We modeled the post-depositional production of ^{10}Be atoms ($[N]_p$) for each sample separately, as each sample has a different burial history. For each sample, time zero (t_0) corresponds to the time at which the sediment is deposited. Considering a progressive burial of 10 cm (Δ_b), time i (necessary to progressively deposit 10 cm) is function of the sedimentation rate at which the material is deposited (S_i):

$$t_i = \frac{\Delta_b}{S_i}. \qquad (1)$$

At the same time, the material deposited at t_0 is now at a depth (Z_i) of

$$Z_i = Z_{i-1} + \Delta_b. \qquad (2)$$

We can now calculate the production rate at Z_i following the model of Schaller et al. (2002), and determine the ^{10}Be produced after deposition ($[N]_p$) as

$$[N]_p = \sum_{i=0}^{d} P(Z_i) * t_i \qquad (3)$$

where i varies with 10 cm steps and represents the cumulative depth at which the sediment has been progressively buried, while d is the actual sample's depth. This value is then scaled for altitude and latitude of the Zielbach catchment and is used for the calculation of the inherited concentration, as explained in the text. The results are shown in Table A2.

The sedimentation rate, based on a 10 cm interval (S_i), is derived from the calculated sedimentation rate for the Adige River (Table 3 in the text), following the high-detailed cores' stratigraphy described in Appendix 1. The determination of S_i is complicated by the presence of interbedded Zielbach deposits (with unknown sedimentation rate), which sometimes isolate thin layers of Adige deposits where the sedimentation rate is unknown. To solve this problem, we assume that the Zielbach sediment is deposited within 1 year (i.e. as an unique debris flow event) assigning a sedimentation rate that correspond to the thickness of the deposit itself (e.g. a Zielbach sequence of 1 meter-thick deposited within 1 year gives a sedimentation rate of 1000 mm/yr). For the thin layers of Adige deposits with unknown sedimentation rate we assigned a value that corresponds to the weighted-average sedimentation rate calculated for the entire core (value of 2.44 mm/yr for core KB11 and 5.19 mm/yr for core KB08). This approach gives us the minimum number of ^{10}Be atoms produced after deposition (minimum $[N]_p$), since it is unlikely that the Zielbach-type sequences are always representative of an unique event (i.e. our

model may assume a too fast burial when a Zielbach-type sequence is present in the core). Consequently, our calculated inherited values are generally overestimating the real inheritance (note that this leads to a conservative underestimation of inferred the paleo-denudation rates). However, this is only true for the KB11 samples, since core KB08 is not influenced by the sedimentation of the Zielbach torrent. The good agreement between the results of KB11 and KB08 allows us to consider our approach reliable also for the KB11 samples.

Table A2. ^{10}Be concentrations ($[N]_{in}$) corrected for fast (min and max ages) and slow burial. $[N]_p$ represents the post-deposition ^{10}Be production.

		Fast Burial (minimum age)			Fast Burial (maximum age)			Slow Burial		
Sample	Depth [cm]	$[N]_p$	$[N]_{in}$	1σ	$[N]_p$	$[N]_{in}$	1σ	$[N]_p$	$[N]_{in}$	1σ
		*10^3 [atoms/gr/yr]			*10^3 [atoms/gr/yr]			*10^3 [atoms/gr/yr]		
KB11-Be1	265	0.000	14.918	1.940	1.329	13.589	1.855	0.001	14.917	1.940
KB11-Be2	732	0.372	40.528	3.160	0.636	40.265	3.150	2.086	38.814	3.095
KB11-Be3	810	0.342	37.374	3.134	0.584	37.131	3.123	0.721	36.995	3.118
KB11-Be4	1230	0.410	2.801	0.771	0.420	2.791	0.770	1.331	1.880	0.674
KB11-Be5	2305	0.289	1.321	0.624				0.665	0.945	0.559
KB11-Be6	3245	0.191	1.451	0.859				0.285	1.357	0.835
KB08-Be1	2675	0.249	0.791	0.489				0.534	0.507	0.433

FIGURE A. CLIMATIC OSCILLATION IN THE EUROPEAN ALPS

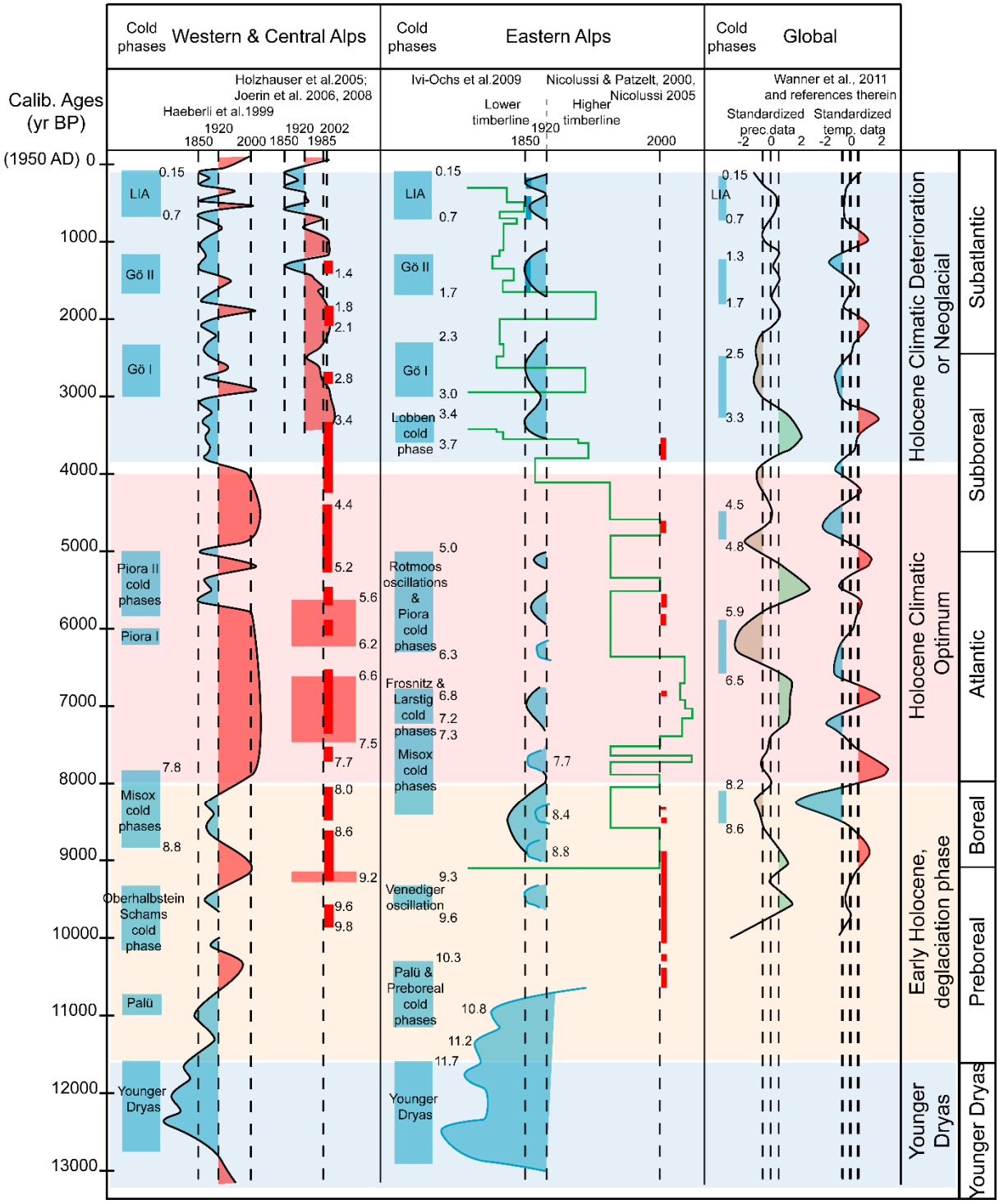

Figure A. Cold and warm climatic intervals reconstructed for the Holocene in the European Alps, with chronozones and main Holocene climatic intervals. During the Holocene Climatic Optimum the glaciers advances only affected small glaciers at high altitude (Ivy-Ochs et al., 2009). Haemberli et al. (1999) analyzed the glacier mass balance and identified cold and warm periods for the Western Alps. Holzhauser et al. (2005) show the variation of the Aletsch glacier (central Switzerland) in the last 3,500 yrs. Joerin et al. (2006 and 2008) and Nicolussi and Patzelt (2000) recognized warm intervals on the basis of subfossil wood found at the base of several glaciers in the Swiss Alps. Ivy-Ochs et al. (2008 and 2009) reconstructed glacier advances based on the ages of erratic boulders on moraines for several

glaciers of the central-eastern Alps. Nicolussi et al. (2005) inferred warm intervals reconstructing the timberline in glaciated catchments of the Austrian Alps and Wanner et al. (2011) gave a global model for the climatic changes of the Holocene based on solar insolation, North Atlantic air circulation, volcanic activity and others fluctuations. Pollen chrono-zones comes from Mangerud et al., 1974; Ravazzi 2003; Ortu et al., 2008.

REFERENCES

Haeberli W., Frauenfelder R., Hoelzle M., Maisch M., 1999. On rates and acceleration trends of global glacier mass changes. Geografiska Annaler, v. 81 A, p. 585-591.

Holzhauser H., Magny M., Zumbuühl H.J., 2005. Glacier and lake-level variations in west-central Europe over the last 3500 years. The Holocene, v. 15, p. 789.

Ivy-Ochs S., Kerschner H., Reuther A., Maisch M., et al., 2006. The timing of glacier advances in the northern European Alps based on surface exposure dating with cosmogenic ^{10}Be, ^{26}Al, ^{36}Cl, and ^{21}Ne. Geological Society of America, special Paper 415.

Ivy-Ochs S., Kerschner H., Reuther A., Preusser F., Heine K., Maisch M., Kubik P.W., Schlüchter C., 2008. Chronology of the last glacial cycle in the European Alps. Journal of Quaternary Science, v. 23, p. 559-573.

Ivy-Ochs S., Kerschner H., Maisch M., Christl M., Kubik P.W., Schlüchter C., 2009. Latest Pleistocene and Holocene glacier variations in the European Alps. Quaternary Science Reviews, v. 28, p. 2137-2149.

Joerin, U.E., Stocker, T.F., Schlüchter, C., 2006. Multicentury glacier fluctuations in the Swiss Alps during the Holocene. The Holocene v. 16, no. 5, p. 697–704.

Joerin U.E., Nicolussi K., Fischer A., Stocker T.F., Schlücter C., 2008. Holocene optimum events inferred from the subglacial sediments at Tschierva Glacier, Eastern Swiss Alps. Quaternary Science Reviews, v. 27, p. 337-350.

Mangerud J., Andersen S.T., Berglund B.E., Donner J.J. 1974. Quaternary stratigraphy of Norden, a proposal for terminology and classification. Boreas, v. 3, p. 109-128.

Nicolussi, K., Patzelt, G., 2000. Discovery of early-Holocene wood and peat on the forefield of the Pasterze Glacier, Eastern Alps, Austria. The Holocene, v. 10, no. 2, p. 191.

Nicolussi, K., Kaufmann, M., Patzelt, G., van der Plicht, J., Thurner, A., 2005. Holocene tree-line variability in the Kauner Valley, Central Eastern Alps, indicated by dendrochronological analysis of living trees and subfossil logs. Vegetation History and Archaeobotany, p. 221–234.

Ortu E., Peyron O., Bordon A., Louis de Beaulieu J., Siniscalco C., Caramiello R., 2008. Lateglacial and Holocene climate oscillations in the South-western Alps: an attempt at quantitative reconstruction. Quaternary International, v. 90, p. 71-88.

Ravazzi C., 2003. An overview of the Quaternary continental stratigraphic units based on biological and climatic events in Italy. Italian Journal of Quaternary Sciences, v. 16, p. 11-18.

Schaller, M., von Blanckenburg, F., Veldkamp, A., Tebbens, L.A., Hovius, N., Kubik, P.W., 2002. A 30000 yr record of denudation rates from cosmogenic ^{10}Be in Middle European river terraces. Earth Planetary Science Letters, v. 204, p. 307–320.

Wanner H., Solomina O., Grosjean M., Ritz S.P., Jetel M., 2011. Structure and origin of Holocene cold events. Quaternary Science Reviews, v. 30, p. 3109-3123.